Surface Soil Moisture Retrieval From L-Band Radiometry: A Global Regression Study

Thierry Pellarin, Jean-Christophe Calvet, and Jean-Pierre Wigneron, *Member, IEEE*

***Abstract*—Using a global simulation of L-band (1.4 GHz) brightness temperature (T_B) for two years (1987 and 1988), the relationship between L-band brightness temperatures and surface soil moisture was analyzed using simple regression models. The global T_B dataset describes continental pixels at a half-degree spatial resolution and accounts for within-pixel heterogeneity, based on 1-km resolution land cover maps. Two different statistical methods were investigated. First, a single regression model was obtained using a linear combination of T_B indexes. This method consisted in retrieving surface soil moisture using the same global regression model for all the pixels. Second, a regression model was calibrated over each pixel using similar linear combinations of the T_B indexes. In both cases, the influence of the radiometric noise on T_B was investigated. Applying these two methods, the capability of L-band T_B observations to monitor surface soil moisture was evaluated at the global scale and during a two-year time period. Global maps of the estimated accuracy of the soil moisture retrievals were produced. These results contribute to better define the potential of the observations from future spaceborne missions such as the Soil Moisture and Ocean Salinity (SMOS) mission.**

***Index Terms*—Global scale, L-band radiometry, soil moisture.**

I. Introduction

THE SURFACE soil moisture is a quantity resulting from the water and energy exchanges at the land-surface/atmosphere interface. Measuring this variable has potential applications in hydrology and meteorology [1], [2]. In particular, time series of surface soil moisture can be employed to retrieve the root-zone soil moisture by using an assimilation algorithm [3]. Soil moisture is highly variable both spatially and temporally in the natural environment, as the result of the heterogeneity of soil properties, topography, land cover, rainfall, and evapotranspiration. Remotely sensed data can provide frequent and spatially comprehensive estimates of the land surface characteristics. The use of remote sensing to map soil moisture arose a large interest. In particular, previous research has shown that L-band passive microwave remote sensing observations can be used to monitor soil moisture over large areas and with a good temporal frequency [4]–[6]. The Soil Moisture and Ocean Salinity (SMOS) mission is a remote sensing project [7] based on a deployable L-band array antenna. SMOS is the second Earth Explorer Opportunity Mission of the European Space Agency (ESA) and is currently studied in Phase B, for a scheduled launch in 2006. The main objective of this mission is to deliver key state variables of land surfaces (soil moisture fields) and of ocean surfaces (sea surface salinity fields) with a ground resolution of 50 km at the swath edges. The radiometer would enable a frequent (three-day revisit) and global coverage, and provide dual polarization and multiangular observations.

Based on large-scale airborne experiments over agricultural sites or ground-based experiments over crop fields, the potential of the passive observations has been evaluated, and retrieval algorithms have been proposed [8]–[11]. Also, a specific sensitivity study on the SMOS view angle configuration was made in [12]. However, as extensive L-band observations from spaceborne systems are not currently available, these different soil moisture retrieval approaches could not be assessed at the global scale. In the present study, we used a global dataset of synthetic brightness temperatures (T_B) at L-band developed by Pellarin *et al.* [13] for a two-year period (1987 and 1988). This period presents a significant climatic variability: contrasting El Niño and La Niña climatic conditions prevailed in 1987 and 1988, respectively. The T_B observations were simulated at the half-degree resolution, for various land surface types (different forests, herbaceous canopies, bare soils, and crops) and for a variety of climatological conditions encountered at the global scale, including soil freezing and the presence of snow. Pixel heterogeneity was accounted for in the T_B simulations.

The obtained synthetic global T_B dataset constitutes a useful reference to develop and validate methods to retrieve soil moisture in the framework of future spatial missions such as SMOS. Based on these T_B data, the objective of the present study was to test simple statistical regression algorithms for surface soil moisture retrieval. Two different statistical methods were investigated. The first approach [referred to as the global regression model (GRM)] consisted in applying a single regression model to retrieve the surface soil moisture over all the continental areas. In the second approach [referred to as the local regression model (LRM)] independent regression models were calibrated over each pixel. The evaluation and the comparison of these methods was made at the global scale for the contrasting 1987 and 1988 years. The accuracy of the soil moisture retrievals was assessed for both years and for various regression approaches. Different values of the instrumental noise are possible for SMOS, depending on the measurement configuration and on the treatment applied to the raw T_B values [14]. A simple statistical processing making best use of the measurement redundancy is likely to reduce the effect of the radiometric noise on the multiangular signature of the land surfaces. Therefore, the 1-K noise level was considered as the reference value

Manuscript received July 17, 2002; revised February 27, 2003. This work was supported by a grant from the European Space Agency (ESA) and the Centre National d'Etudes Spatiales (CNES).

T. Pellarin and J.-C. Calvet are with Météo-France, CNRM/GAME, URA CNRS 1357, 31057 Toulouse Cedex 1, France.

J.-P. Wigneron is with INRA/Bioclimatologie, 33883 Villenave d'Ornon, France.

Digital Object Identifier 10.1109/TGRS.2003.813492

of measurement error in this study. However, the influence of different instrumental noise levels on T_B (1, 2, and 3 K) was evaluated.

Using state-of-the-art simulations, the results presented in this study provided an evaluation of the SMOS capability to estimate surface soil moisture at the global scale and during a two-year period. The global dataset including simulated surface soil moisture and brightness temperatures is presented in Section II. A general description of the statistical approaches is given in Section III. Finally, GRM and LRM are assessed in Sections IV and V, respectively.

II. Simulated Surface Soil Moisture and Synthetic T_B

In this study, a global dataset was used, including synthetic L-band brightness temperatures and the land surface characteristics during a two-year period from January 1, 1987 to December 31, 1988. A detailed description of the dataset and of the modeling approaches used to carry out the simulations was given in Pellarin *et al.* [13]. The main features of the dataset are summarized in this section. The simulations were based on a two-step process. First, a land surface scheme, the Interactions between Soil, Biosphere and Atmosphere (ISBA) model [15], was used at the global scale to simulate the time variations of the surface state characteristics (i.e., the soil temperature and moisture content at the surface and at depth, the snow cover characteristics) required by the L-band emission model. The ISBA simulations used a two-year atmospheric forcing derived from the International Satellite Land Surface Climatology Project Initiative I (ISLSCP I) data [16] of the Global Soil Wetness Project (GSWP), and on a detailed global surface database (ECOCLIMAP [17]), containing a global land cover map at a spatial resolution of 1 km. Second, the simple L-band Microwave Emission of Biosphere model (L-MEB), based on the radiative transfer equations, was used to produce multitemporal T_B maps from the ISBA outputs as well as from information derived from the thematic maps and the atmospheric forcing database. The brightness temperatures were computed at five different incidence angles (0°, 20°, 30°, 40°, and 50°) and two polarizations (H and V).

The synthetic L-band T_B were simulated at the half-degree resolution, and the subpixel heterogeneity was accounted for by using a "multipatch" version of ISBA. This version is able to simulate distinct water and energy budgets in the same pixel for the three principal land covers that were considered in this study (namely bare soil, woody vegetation, and herbaceous vegetation). The simulation of T_B for the heterogeneous pixels included different stages involving the ISBA multipatch model and L-MEB (a dataflow chart showing how the dataset was generated is presented in [13]).

First, the ISBA multipatch model was run at a spatial resolution of half a degree (about 50×50 km^2) and produced daily 0600 and 1800 local standard time (LST) maps of the variables (surface soil moisture and temperature, and snow characteristics) required for running the L-MEB model. A number of variables produced by ISBA or derived from the ISLSCP I and ECOCLIMAP datasets were stored daily for the two considered local times. These variables are listed in Table I. For a given pixel, distinct simulations of the same variable were performed by ISBA, for all the patches included in the pixel.

TABLE I
Main Input Variables of the L-Band Microwave Emission of Biosphere Model (L-MEB)

Variables	Description	Unit
T_{AIR}	Air temperature (2m)	K
T_S	Surface soil temperature	K
T_2	Soil temperature	K
wg	Surface soil moisture	$m^3 m^{-3}$
wg_I	Surface iced soil moisture	$m^3 m^{-3}$
w_R	Rain interception by the canopy	$kg m^{-2}$
h_{SNOW}	Snow depth	m
ρ_{SNOW}	Snow density	$kg m^{-3}$
T_{SNOW}	Snow temperature	K
$w_{SNOWliq}$	Liquid water content of snow cover	$kg m^{-2}$
LAI	Leaf Area Index	$m^2 m^{-2}$

Second, the surface-state maps produced by ISBA, and the leaf area index (LAI) and air temperature data derived from the ECOCLIMAP and ISLSCP I databases, were employed to run the L-MEB model. The vegetation module of L-MEB is derived from the $\tau - \omega$ approach (e.g., see Wigneron *et al.* [9]), associated with a snow emission model developed by Pulliainen *et al.* [18], and a simple parameterization of the atmospheric effects [13]. The main variables needed to simulate T_B are the surface soil moisture and temperature, the vegetation water content, the soil roughness parameters, the soil type, and the snow mantel characteristics (depth, density, grain size, liquid water content). The air temperature and the altitude are also needed to simulate the atmospheric effects. The simulation process also accounts for subpixel heterogeneity. Four main surface types, and the associated values of their cover fraction within each pixel, are considered in the L-MEB simulations: bare soil, herbaceous vegetation (grassland or crops), forests (coniferous, broadleaf or tropical forests), and open water surfaces (lakes, river, etc.).

For all the land cover types, snow was considered. It was assumed that snow covers bare soil and herbaceous vegetation surfaces. For forests, it was considered that the snow layer was below the forest canopy. Situations of partially and/or totally frozen soil was accounted for by using different values of the soil dielectric permitivity. Also, open water surfaces could be frozen at the surface (in this case, the dielectric permitivity of ice was used). The brightness temperature of the mixed pixel including all (or some of) the four surface types was written as

$$T_{Bp} = f_B \cdot T_{Bp-B} + f_F \cdot T_{Bp-F} + f_H \cdot T_{Bp-H} + f_W \cdot T_{Bp-W} \tag{1}$$

where f_X and T_{Bp-X} are the cover fraction and the p-polarized brightness temperature of the different surface types ($X = B$ for bare soil, $X = F$ for forests, $X = H$ for herbaceous vegetation-covered surfaces, and $X = W$ for open water sur-

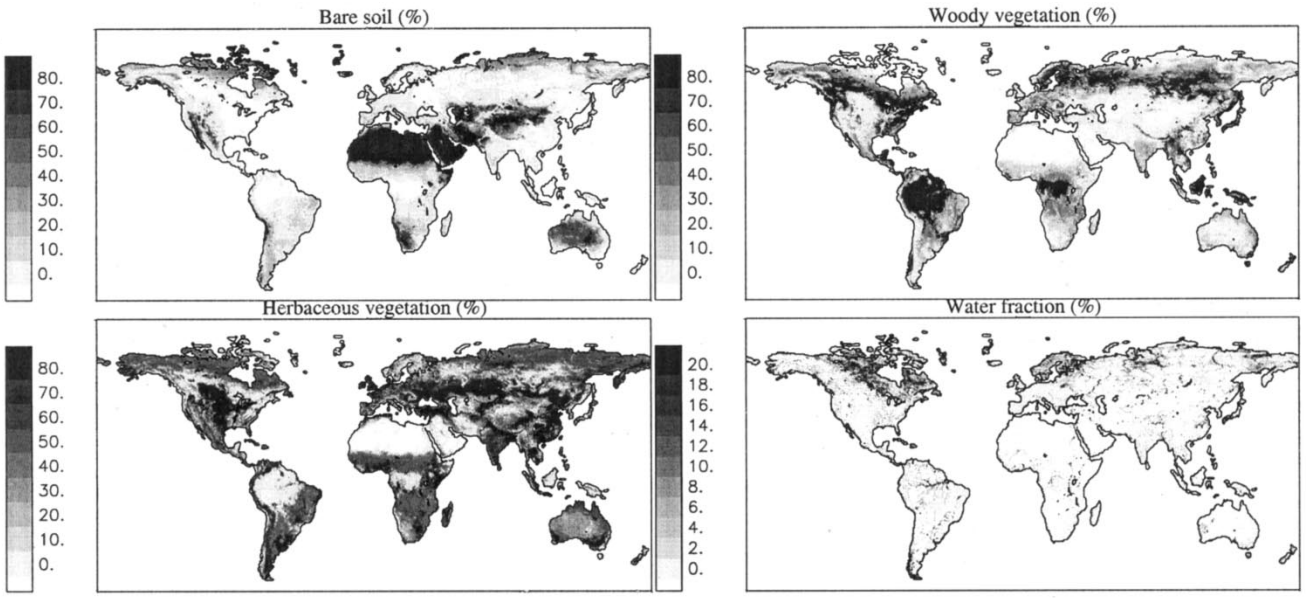

Fig. 1. Global half-degree maps obtained from the ECOCLIMAP dataset. Fractional cover of bare soil, woody vegetation, herbaceous vegetation, and free water surfaces.

faces). The modeling of T_{Bp-X} also included the reflection of the down-welling sky and cosmic radiation by the surface.

For herbaceous vegetation, either grasslands or crops were considered. Mixed grassland and crop cover was not considered. In the same way, only one forest type (coniferous, broadleaf, or tropical forests) was regarded on a given pixel, and this type corresponded to the largest forest-type cover fraction derived from ECOCLIMAP. For all the vegetation types, the $\tau - \omega$ L-band emission model is based on the vegetation single-scattering albedo ω representing the scattering within the canopy layer and on the vegetation optical depth τ, which parameterizes the attenuation effects. The vegetation optical depth τ can be estimated as follows using the so-called b parameter [19]:

$$\tau = b\mathrm{VW}_C \tag{2}$$

where VW_C (in kilograms per square meter) is the above-ground vegetation water content.

As far as the b parameter is concerned, a value of 0.12 ± 0.03 was found to be representative of most agricultural crops at 1.4 GHz [19]. In the present study, for nonforested canopies, VW_C was related to the LAI as $\mathrm{VW}_C = 0.5$ LAI. It follows that the optical depth of the low vegetation canopies varies with time like the monthly estimates of LAI derived from the ECOCLIMAP database. On the contrary, over forests, the value of τ was assumed to be constant and was related to the branch water content [20]. The vegetation parameters of all the vegetation types considered in this work are given in Table II. The highest optical depth was prescribed for tropical forest (τ was set equal to two for this vegetation type). The spatial distribution of the different land covers is shown in Fig. 1. Most pixels are heterogeneous, since only 10% of them consist of a single cover type (mainly bare soil in Sahara). In ECOCLIMAP, the total forest area represents 29.2% of the continental surface (9.6% of tropical forest, 5.2% of broadleaf forest, and 14.4% of coniferous forest). Herbaceous vegetation represents 47.3% of the continental surface (12.9% of crops and 34.4% of grassland). Finally, the bare soil surface type covers 23.5% of the continental areas. It can be also noted that for more than 33% of the pixels, the surface fraction of open water exceeds 1%.

TABLE II
VEGETATION PARAMETERS OF L-MEB

Surface Type	single scattering albedo ω	b parameter	Vegetation Water Content *VWc*
Grasslands	0.05	0.2	0.5 LAI (kg m^{-2})
Crops	0.05	0.15	0.5 LAI (kg m^{-2})
Rainforests	0.15	0.33	6 kg m^{-2} (branches)
Deciduous forests	0.15	0.33	4 kg m^{-2} (branches)
Coniferous forests	0.15	0.33	3 kg m^{-2} (branches)

III. A STATISTICAL APPROACH: GENERAL METHODOLOGY

To retrieve surface soil moisture (wg) from the microwave brightness temperature, three main types of approaches can be found in the literature: 1) establishing a direct relationship between T_B and soil moisture [4], [6], 2) inversion of a forward model [9]–[12], or 3) using a neural network [21]. In this study, the first retrieval approach, based on simple regression models, was investigated using the large dataset described in the previous section.

The easiest way to obtain a relationship between *wg* and the L-band signal is to search for direct empirical relationships on the type

$$wg^* = a_0 + a_1 T_{B1} + a_2 T_{B2} + \cdots + a_q T_{Bq} \tag{3}$$

TABLE III
DEFINITION OF THE INDEXES USED IN THIS STUDY. THE SUBSCRIPTS p, θ, AND β DENOTE THE POLARIZATION (V OR H) AND TWO DIFFERENT INCIDENCE ANGLES, RESPECTIVELY

Index	Name	Definition
$AR_{p,\theta,\beta}$	Angular Ratio	$\frac{T_{B(p,\theta)}}{T_{B(p,\beta)}}$
PR_{θ}	Polarization Ratio	$\frac{T_{B(V,\theta)}-T_{B(H,\theta)}}{T_{B(V,\theta)}+T_{B(H,\theta)}}$
$PD_{p,\theta}$	Polarization Difference	$\left[T_{B(V,\theta)}-T_{B(H,\theta)}\right]T_{B(p,\theta)}$
$AD_{p,\theta,\beta}$	Angular Difference	$T_{B(p,\theta)}-T_{B(p,\beta)}$

where T_{Bi}, $i = 1 \cdots q$, correspond to brightness temperatures obtained for various configurations of the sensor, and wg^* is the estimated surface soil moisture.

Relevant results have been obtained using this method [4], [6]. However, when multiconfiguration observations are available (multiangular or dual-polarization data), a slightly different approach consists in using different "indexes" that are computed from the T_{Bi} data and which are known to be related to the land surface characteristics [22]–[25]. This approach has been chosen in the present work. The indexes used in this study are defined in Table III. They make use of the multiangular and dual-polarization capability of SMOS that was shown to be useful in the soil moisture retrieval process [12]. The indexes given in Table III can be related to surface characteristics such as soil moisture or vegetation biomass. For example, the modified polarization difference ($PD_{p,\theta}$) and the polarization ratio (PR_{θ}) were found to be good indicators of biomass and of soil wetness [25], respectively. The rationale for using indexes consisting in ratios of T_{Bi} data (AR, PR, or AD) is that these indexes are weakly sensitive to the effect of the land surface temperature [26].

Therefore, the simple regression approach used in this study can be written as

$$wg^* = a_0 + a_1(\mathrm{IND}_1) + a_2(\mathrm{IND}_2) + \cdots + a_q(\mathrm{IND}_q) \quad (4)$$

where a_0, a_1, $\ldots a_q$ are the regression coefficients and IND_0, IND_1, $\ldots \mathrm{IND}_q$ the selected indexes presented in Table III.

The reference surface soil moisture wg which was used in this study was computed for each pixel as

$$wg = \frac{f_B \cdot wg_B + f_F \cdot wg_F + f_H \cdot wg_H}{f_B + f_F + f_H} \quad (5)$$

where f_B, f_F, and f_H represent the bare soil, forest, and herbaceous fractions of the pixel, respectively, and wg_B, wg_F, and wg_H correspond to the soil moisture of the bare soil, forest, and herbaceous fractions of the pixel, respectively.

Regression models are expected to depend strongly on the cover fraction of the different surface types (forest, low vegetation canopy, open water area) within the pixel, and they should be quite different from one pixel to another. Therefore, two main approaches were tested: the global and the local regression model methods (GRM and LRM, respectively). In the first approach, a single regression model was used to retrieve surface soil moisture over all the pixels, while in the second approach independent regression models were calibrated over each pixel.

Before considering the regression between T_B indexes and wg, different noise levels were applied to the T_B data, accounting for instrumental noise and Faraday rotation effects. Instrumental noise was represented by a centered Gaussian distribution with a standard deviation of either 1, 2, or 3 K, which was added to each T_B observation. Preliminary tests showed that the regression models obtained using noise-free T_B data were markedly different from those derived from noisy data. Also, these noise-free regression models were found to be quite inefficient to retrieve soil moisture from noisy T_B data, and for both GRM and LRM, the regression coefficients were found to strongly depend on the noise level on T_B.

The effects of Faraday rotation on the T_B observations were not modeled in L-MEB. Instead, a noise representative of the effects due to the Faraday rotation was accounted for and was added to the synthetic T_B. Faraday rotation tends to depolarize the signal. This polarization mixing effect can be represented by [26]

$$T^*_{BH} = \cos^2(\phi + d\phi)\, T_{BH^+} \sin^2(\phi + d\phi)\, T_{BV} \quad (6a)$$

$$T^*_{BV} = \sin^2(\phi + d\phi)\, T_{BH^+} \cos^2(\phi + d\phi)\, T_{BV} \quad (6b)$$

where T^*_{BH} is the value of T_{BH} after accounting for Faraday effects, and ϕ and $d\phi$ are the angle of Faraday and the error on the estimation of ϕ, respectively. In this study, we assumed that ϕ was close to 0° and that $d\phi$ was a Gaussian noise with a standard variation of 2°. Based on the recent article of Le Vine and Abraham [26], the effect of Faraday rotation on L band varies from location to location, and could amount to as much as 10° to 15°. However, as emphasis will be put on the 0600 A.M. orbit in order to minimize diurnal cycle effects, the expected magnitude of Faraday rotation is at most 5°. Then, it does not seem unreasonable to assume that external information, e.g., derived from global positioning system data, will provide an estimate of the vertical electron content within better than 30% to 40%. This is the rationale for assuming a 2° Faraday rotation error. In addition, in the SMOS case, using full polarization data might allow a direct estimation of the Faraday rotation through making use of the third Stokes parameter, as suggested by Yueh [27]. This issue is being studied presently. In this study, typical differences between T^*_{Bp} and T_{Bp} over land do not generally exceed 0.1 K. Errors on T_B due to an uncertainty of 2° on the Faraday angle are lower than 0.5 K with a probability of 98%.

To evaluate the accuracy of the soil moisture retrievals, four criteria characterizing the difference between the reference (wg) and estimated (wg^*) values of soil moisture were used: the correlation coefficient (R^2), the efficiency (E), the root mean square error (rms), and the mean bias (MB).

TABLE IV
REGRESSION COEFFICIENTS OF GRM (8) AND THE ASSOCIATED REGRESSION SCORES: SQUARE CORRELATION COEFFICIENT (R^2), ROOT MEAN SQUARE ERROR (RMS), MEAN BIAS (MB)—ESTIMATES MINUS REFERENCE—CALCULATED ON EIGHT × 56 356 POINTS (EIGHT DATES WERE CONSIDERED)

noise	a_0	a_1	a_2	a_3	R^2 (-)	RMS ($m^3\ m^{-3}$)	MB ($m^3\ m^{-3}$)
1K	-4.73108	-1.47312	2.49360	2.41251	0.55	0.075	0.035
2K	-3.77086	-0.564238	1.67815	2.26879	0.47	0.081	0.008
3K	-2.86064	-0.481112	1.18256	1.85686	0.39	0.088	0.005

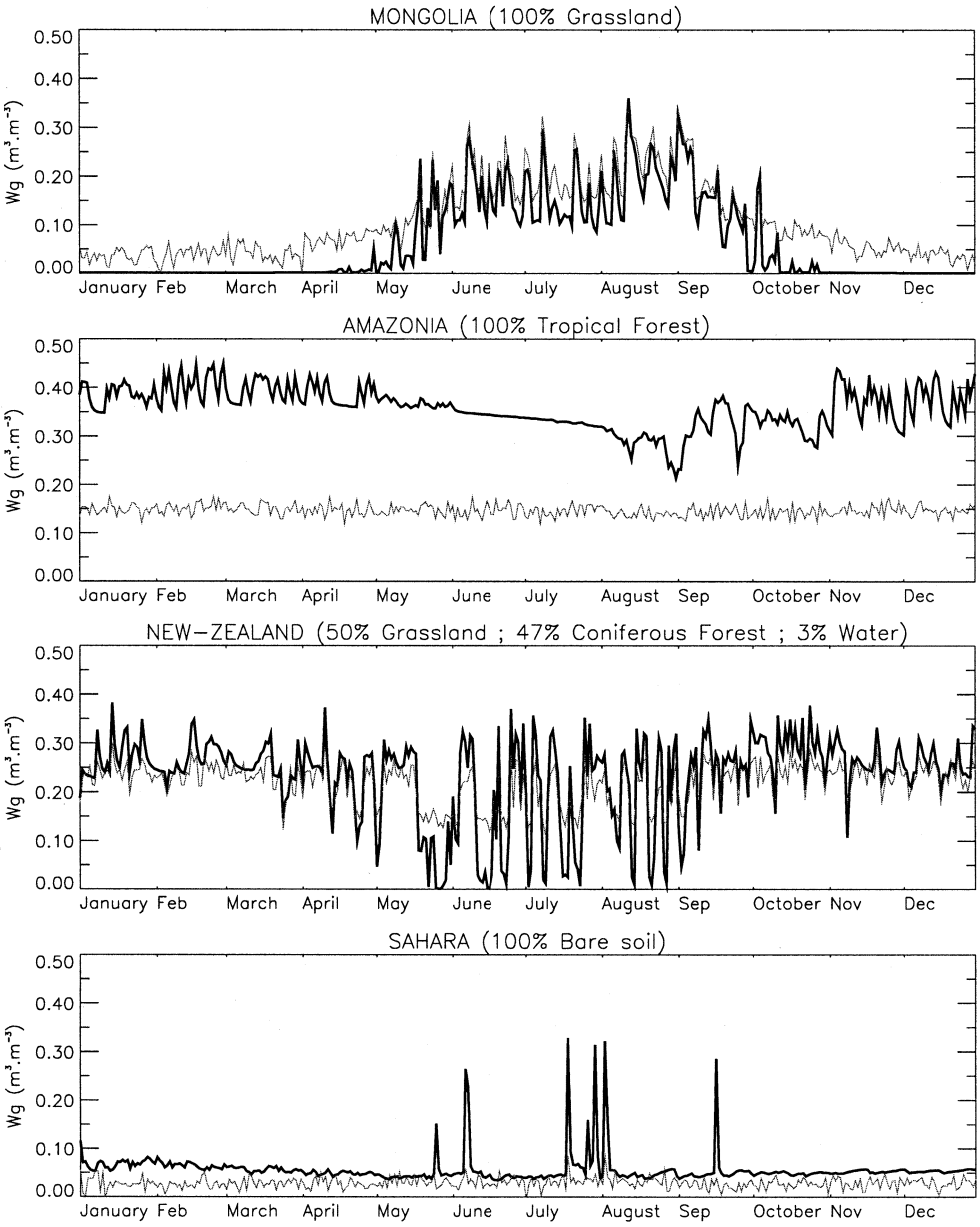

Fig. 2. Four examples of the annual time variations of the reference and GRM-estimated surface soil moisture (thick and thin lines, respectively), for a 1-K noise level, in 1988, at 0600 LST.

The efficiency (or skill score) was defined as

$$E = 1 - \left[\frac{\sum_i (wg_i - wg_i^*)^2}{\sum_i (wg_i - \mu)^2} \right], \qquad \text{with } \mu = \frac{1}{N} \sum_{i=1}^{N} wg_i \quad (7)$$

where wg_i and wg_i^* represent reference and retrieved surface soil moisture values, respectively. μ is the mean value of the reference values. Positive values of E indicate that the employed regression model is more informative than prescribing a constant value of wg equal to μ.

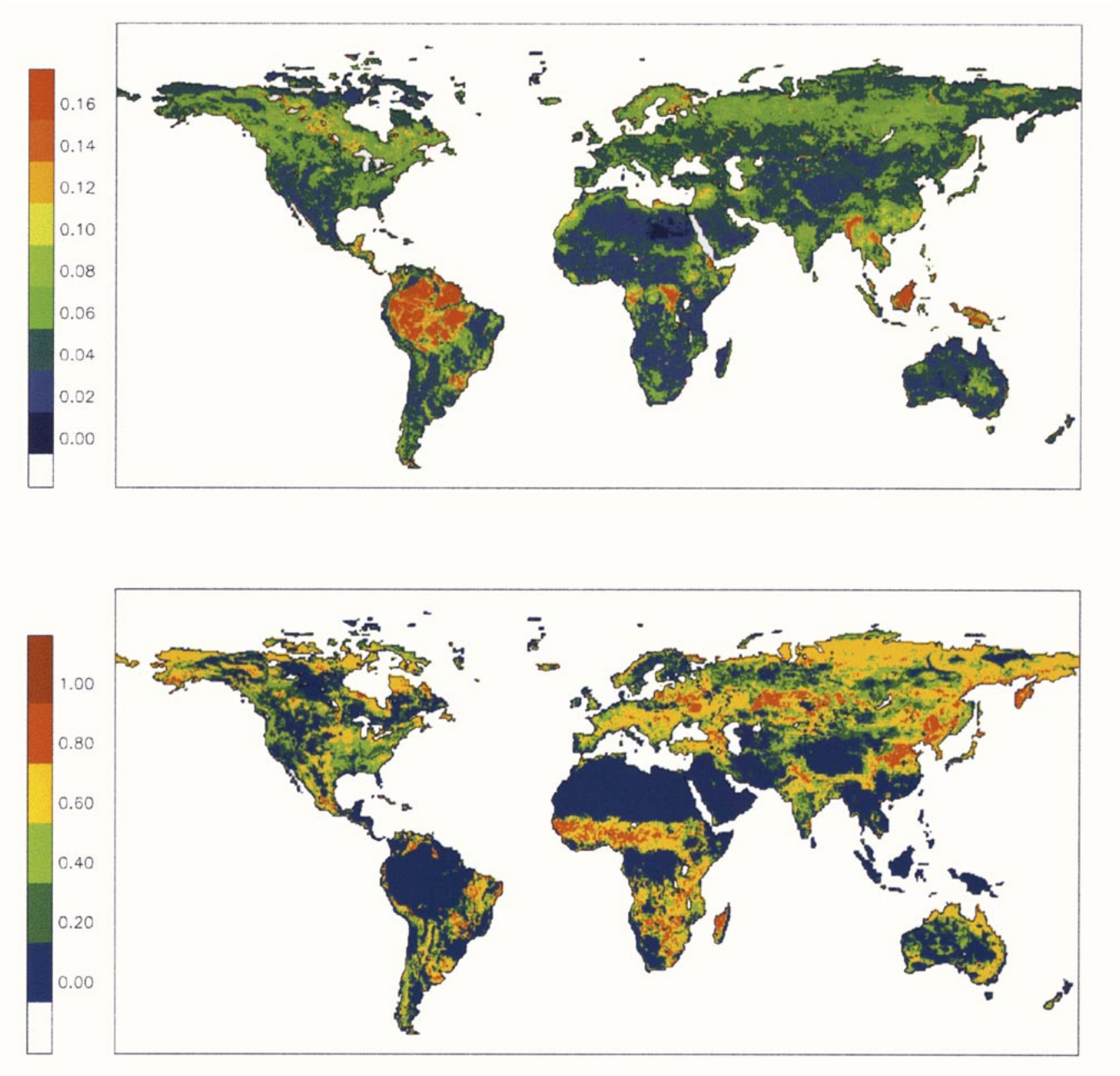

Fig. 3. Spatial distribution of the GRM (8) scores for a 1-K noise level, in 1988, at 0600 LST. (Top) Root mean square error. (Bottom) Model skill score.

IV. GRM

A. Index Selection

A preliminary analysis was performed for a few days in order to select best suited indexes for soil moisture retrieval. Because of the large number of pixels, the regressions were performed on eight global maps corresponding to different days of 1987. The selected days were February 1, May 1, August 1, and November 1, respectively, at 0600 and 1800 LST. The chosen days encompassed different seasons and different times of the day in order to obtain a training dataset representative of the global surface soil moisture variability. The objective was to analyze 1) the relevance of each index for soil moisture retrieval and 2) the influence of the number of indexes employed in the regression model on the accuracy of retrieved wg^* values. Numerous combinations of the indexes given in Table III were tested in the retrieval process of wg.

Using only one index, a linear regression using $\mathrm{AR}_{H,\,50,\,20}$ provided the best results in terms of rms error. With two indexes, a linear regression using $\mathrm{AD}_{V,\,50,\,40}$ and $\mathrm{AR}_{H,\,50,\,20}$ performed best. Best results with three indexes were obtained by using the polarization ratio (PR_{θ}) and two angular ratios corresponding to vertical and horizontal polarizations ($\mathrm{AR}_{V,\,\theta,\,\beta}$ and $\mathrm{AR}_{H,\,\theta,\,\beta}$, respectively). Vegetation biomass and soil moisture strongly affect the magnitude of the land surface microwave emission, but also the dependence of emissivity on incidence angle and polarization. The indexes PR_{θ}, $\mathrm{AR}_{V,\,\theta,\,\beta}$, and $\mathrm{AR}_{H,\,\theta,\,\beta}$, can be used to parameterize this dependence. The retrieval accuracy, in terms of rms error, was investigated for various combinations of the indexes used in GRM, for different instrumental noise levels:

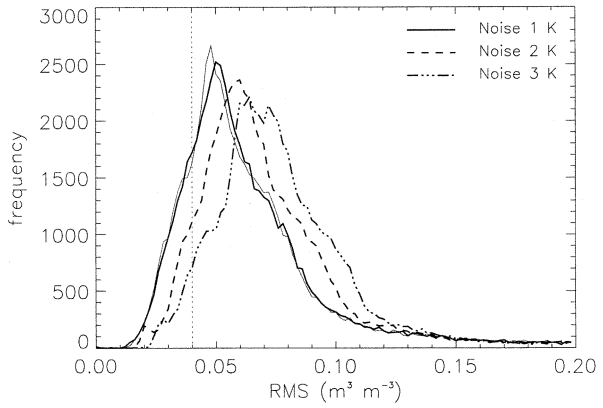

Fig. 4. Probability density function of the global rms error on the retrieved surface soil moisture, at 0600 LST, using GRM (8) for a 1-K noise level in 1987 and 1988 (thin and thick lines, respectively) and for a 2- and 3-K noise level in 1988 for all continental pixels. The dotted vertical line represent the 0.04 $m^3 \cdot m^{-3}$ threshold value.

1, 2, and 3 K. It was concluded that whatever the prescribed T_B noise level, using more than three indexes in the wg^* regression model does not improve the retrieval accuracy.

In order to check whether the choice of different days could produce the same optimal indexes, another eight-day selection was considered (i.e., the tenth instead of the first of each of the four months). This new run led to the same index choice and to similar regression coefficients and scores. Besides, it was checked that the use of additional global maps (i.e., more than the eight selected days of 1987) did not improve the performance of GRM. Finally the three indexes PR_θ, $AR_{V,\theta,\beta}$, and $AR_{H,\theta,\beta}$, which provided the best results in the preliminary tests, were used to build the regression models of GRM. Preliminary results (not shown) indicated that using the incidence angles $\theta = 0^\circ$ and $\beta = 50^\circ$ in $AR_{V,\theta,\beta}$ and $AR_{H,\theta,\beta}$ provides the best results. However, it is expected that nadir-viewing will be obtained for only a small part of the SMOS field of view, and $\theta = 20^\circ$ was used instead of $\theta = 0^\circ$.

The GRM regression model, based on T_B measurements at $\theta = 20^\circ$ and $\theta = 50^\circ$ for both polarizations, was written as

$$wg^* = a_0 + a_1 PR_{40} + a_2 AR_{V,50,20} + a_3 AR_{H,50,20} \quad (8)$$

where a_0, a_1, a_2, and a_3 are the regression coefficients.

Whatever noise level, if a single regression model is used over the whole continental areas, the obtained average rms score is always higher than the desired 0.04 $m^3 \cdot m^{-3}$ accuracy for wg^* (the 0.04 $m^3 \cdot m^{-3}$ threshold was considered as the required accuracy for studies over land in the SMOS mission [7], [12]).

B. GRM Results for 1987 and 1988

The regression coefficients of (8), obtained for different noise levels, are given in Table IV [the method was referred to as GRM (8)]. GRM (8) was applied at the global scale for both 1987 and 1988. The comparison between the time variations in retrieved and reference surface soil moisture (wg^* and wg, respectively) is presented in Fig. 2 over four selected pixels, in 1988, for a T_B noise of 1 K. The first pixel, located in the Mongolian plain, consists of a homogeneous herbaceous area (100% of its surface is composed of grasslands). The second one is entirely covered with tropical forest and is located in Amazonia. The third one is a mixed pixel located in New Zealand and is composed of 50% of grassland, 47% of coniferous forest, and 3% of water. The last one is a 100% bare soil pixel located in the Saharan desert. In the first plot (Mongolian plain), the reference surface soil moisture is close to zero from November to April. There is no liquid water at the soil surface because of soil freezing. It can be seen that the GRM method was not able to correctly represent the time variations of the soil moisture during the winter period. Over the whole year, the rms is 0.047 $m^3 \cdot m^{-3}$, and the efficiency is 0.71. Over the Amazon forest pixel, soil moisture cannot be retrieved. The rms error is 0.213 $m^3 \cdot m^{-3}$ and the efficiency is negative. In this case, the optical thickness of this dense vegetation canopy is high ($\tau \approx 2$), and the nearly opaque canopy masks the soil emission so that T_B is almost insensitive to soil moisture change. Over the third pixel (New Zealand), several short freezing periods occurred from May to September, and as for the Mongolian pixel, soil moisture cannot be retrieved when the soil is frozen (rms error = 0.055 $m^3 \cdot m^{-3}$). Over the last pixel (in the arid Saharan region), the computed rms error is relatively low (0.042 $m^3 \cdot m^{-3}$), but the computed efficiency is negative (-0.590) because of a large bias. Moreover, the retrieval method could not detect the few soil moisture rises due to rainfall events in 1988.

The results of the comparison between the retrieved and the reference surface soil moisture (wg^* and wg, respectively) at the global scale are summarized in Table V. The global yearly scores $\overline{R^2}$, $\overline{E}$, $\overline{rms}$, and $\overline{MB}$ represent the average values of the scores calculated for each land pixel during a one-year period. The retrieving performance is similar for both years, and the $\overline{rms}$ error varies from 0.065–0.078 $m^3 \cdot m^{-3}$, depending on the noise level. These values of the $\overline{rms}$ error are significantly higher than the 0.04 $m^3 \cdot m^{-3}$ required accuracy. In 1988, for a 1-K noise level, the global $\overline{rms}$ error is 0.066 $m^3 \cdot m^{-3}$. In this case, the spatial distribution at the global scale of both the rms errors and the efficiency is given in Fig. 3. In the tropical forest regions such as the Amazonian, African, and Indonesian forests, high rms errors, often greater than 0.1 $m^3 \cdot m^{-3}$, were obtained. Accuracy values better than 0.04 and 0.06 $m^3 \cdot m^{-3}$ were obtained over 16.5% and 54% of the continental surfaces, respectively. The global rms error histogram representing the GRM (8) soil moisture retrievals for both 1987 and 1988 years is given in Fig. 4 (solid lines). It can be seen that the rms distribution is basically the same for either 1987 or 1988. Histograms related to 2- and 3-K noise levels on T_B are also shown in Fig. 4, showing that the noise level has a detrimental influence on the soil moisture retrieval accuracy. However, the loss in accuracy relative to a noise rise is rather weak (see Table V). At the global scale, the $\overline{rms}$ error increases of about 0.006 $m^3 \cdot m^{-3}$ for each kelvin added to the noise level. The same results were obtained for both 1987 and 1988 years.

C. Improvements of GRM

In the previous section, it was shown that the performance of a global retrieval algorithm is low (below the expected accuracy). To overcome this problem, two methods can be proposed: including the fraction of water within each pixel in the predictor set or excluding from the analysis the areas presenting

TABLE V
GRM (8) SPATIAL MEAN OF THE SCORES ON SOIL MOISTURE RETRIEVALS FOR 1987 AND 1988, AT 0600 LST, FOR THREE NOISE LEVELS (1, 2, AND 3 K): SQUARE CORRELATION COEFFICIENT ($\overline{R^2}$), SKILL SCORE ($\overline{E}$), ROOT MEAN SQUARE ERROR ($\overline{rms}$), MEAN BIAS ($\overline{MB}$)—RETRIEVED MINUS REFERENCE. RMS IS THE GLOBAL ROOT MEAN SQUARE ERROR, BASED ON THE TOTAL SUM OF SQUARES

Year	noise	$\overline{R^2}$ (-)	$\overline{E}$ (-)	$\overline{RMS}$ ($m^3\ m^{-3}$)	RMS ($m^3\ m^{-3}$)	$\overline{MB}$ ($m^3\ m^{-3}$)
1987	1K	0.66	0.358	0.065	0.073	0.000
	2K	0.51	0.264	0.071	0.077	-0.001
	3K	0.40	0.179	0.077	0.083	-0.001
1988	1K	0.67	0.365	0.066	0.073	-0.001
	2K	0.52	0.268	0.072	0.078	-0.001
	3K	0.40	0.181	0.078	0.083	-0.001

TABLE VI
REGRESSION COEFFICIENTS FOR GRM (8) AND THE ASSOCIATED REGRESSION SCORES: SQUARE CORRELATION COEFFICIENT (R^2), ROOT MEAN SQUARE (RMS) ERROR, MEAN BIAS (MB)—ESTIMATES MINUS REFERENCE—CALCULATED ON EITHER $8 \times 50\,720$ OR $8 \times 45\,084$ POINTS (EIGHT DATES WERE CONSIDERED), WITHOUT EITHER 10% OR 20% OF THE PIXELS FOR WHICH GRM PRESENTS THE LARGEST ERRORS, RESPECTIVELY

GRM excluding	noise	a_0	a_1	a_2	a_3	R^2 (-)	RMS ($m^3\ m^{-3}$)	MB ($m^3\ m^{-3}$)
-10% of surfaces	1K	-5.59517	-0.101453	2.80047	2.91462	0.69	0.058	0.007
	2K	-4.43267	0.205171	2.05656	2.50294	0.56	0.068	0.002
	3K	-3.31949	0.0879842	1.49161	1.96203	0.44	0.078	0.008
-20% of surfaces	1K	-5.68176	0.0517677	2.83596	2.95847	0.73	0.052	-0.002
	2K	-4.49072	0.266532	2.09047	2.52222	0.59	0.064	-0.001
	3K	-3.31574	0.106423	1.48927	1.9582	0.46	0.074	0.005

little sensitivity of T_B to soil moisture. The open water surfaces (lakes, rivers, etc.) have a significant influence on the simulated T_B. While most T_B values (H and V polarization, at 40° incidence angle) range between 220 and 270 K over water-free land pixels in our simulations, the pixels including 20% to 50% of open water surfaces display values ranging between 170 and 230 K. This factor may introduce errors in the GRM retrievals over land. An attempt was made to use the water fraction of a given pixel as an additional predictor of surface soil moisture in the regression model. In the ideal situation where the water fraction was known, the average gain of accuracy (not shown) was marginal. Besides, the practical feasibility of using such a version of GRM would be limited by the uncertainties on the fraction of open water surfaces.

Another way to improve GRM methodology consists in discarding the pixels presenting the largest error (e.g., dense forests). These pixels have a great influence on the obtained GRM, which is used over the whole continental areas, and disrupt soil moisture retrieval at the global scale. In order to assess this effect, either 10% or 20% of the continental pixels associated with the higher rms error values were excluded from the GRM calibration. The 10% and 20% eliminated pixels correspond to rms values higher than 0.102 $m^3 \cdot m^{-3}$ and 0.081 $m^3 \cdot m^{-3}$, respectively. These pixels correspond to the dense tropical forests and also to areas where the fractional cover of open water is significant (e.g., Canada and Scandinavia). The regression coefficients for GRM (8) after eliminating 10% and 20% of the "worst pixels" (GRM-10% and GRM-20%, respectively) are given in Table VI. They were obtained by the method presented in Section IV-A. The results in terms of soil moisture retrievals are given in Table VII: the comparison of the regression models is made over several geographical domains covering 100%, 90%, and 80% of the continental surfaces. Direct comparisons between the results of GRM, GRM-10%, and GRM-20% were made for the same set of pixels, namely over the area where GRM-20% was calibrated (i.e., 80% of the continental surfaces). As expected, after eliminating the worst pixels, improved results were obtained for GRM (Table VII). Table VII and Fig. 5 show that GRM-10% and GRM-20% provided better results than GRM. The use of GRM-20% improved only slightly the results in comparison with GRM-10%. Using GRM, the soil moisture retrieval rms error was lower than 0.04 $m^3 \cdot m^{-3}$ over 20.5% of the 80% continental surfaces. This proportion reached 36% and 40% with GRM-10% and GRM-20%, respectively.

V. LRM

The previous section showed that the accuracy of a regression model to retrieve surface soil moisture from T_B indexes can be improved by focusing on certain continental areas. In the extreme, the LRM method uses as many statistical relationships

TABLE VII
COMPARISON OF FOUR REGRESSION MODELS (GRM (8), GRM-10%, GRM-20%, AND LRM (9)) SCORES ON SOIL MOISTURE RETRIEVALS FOR 1988, AT 0600 LST, FOR A 1-K NOISE LEVEL, EXCLUDING 0%, 10%, AND 20% OF THE PIXELS FOR WHICH GRM OR LRM PRESENT THE LARGEST ERRORS: SQUARE CORRELATION COEFFICIENT ($\overline{R^2}$), SKILL SCORE ($\overline{E}$), ROOT MEAN SQUARE ERROR ($\overline{rms}$), MEAN BIAS ($\overline{MB}$)—RETRIEVED MINUS REFERENCE. NOTE THAT SIMILAR RESULTS WERE OBTAINED FOR BOTH 1987 AND 1988 AND THAT RESULTS ARE GIVEN FOR 1988 ONLY. ALSO, THE RESULTS ARE GIVEN ONLY FOR THE 1-K NOISE LEVEL, WHICH IS A REFERENCE NOISE VALUE EXPECTED FOR THE SMOS OBSERVATIONS. RMS IS THE GLOBAL ROOT MEAN SQUARE ERROR, BASED ON THE TOTAL SUM OF SQUARES

Model	Surface	$\overline{R^2}$ (-)	$\overline{E}$ (-)	$\overline{RMS}$ ($m^3\ m^{-3}$)	RMS ($m^3\ m^{-3}$)	$\overline{MB}$ ($m^3\ m^{-3}$)
GRM (8)	100%	0.67	0.36	0.066	0.073	-0.001
GRM (8)	90%	0.70	0.40	0.057	0.060	-0.007
GRM (8)	80%	0.70	0.44	0.053	0.055	-0.007
GRM-10%	100%	-	-	-	-	-
GRM-10%	90%	0.77	0.51	0.051	0.055	-0.001
GRM-10%	80%	0.77	0.54	0.046	0.049	-0.002
GRM-20%	100%	-	-	-	-	-
GRM-20%	90%	-	-	-	-	-
GRM-20%	80%	0.77	0.54	0.046	0.049	0.003
LRM (9)	100%	0.78	0.76	0.030	0.032	0
LRM (9)	90%	0.82	0.81	0.029	0.031	0
LRM (9)	80%	0.83	0.81	0.029	0.030	0

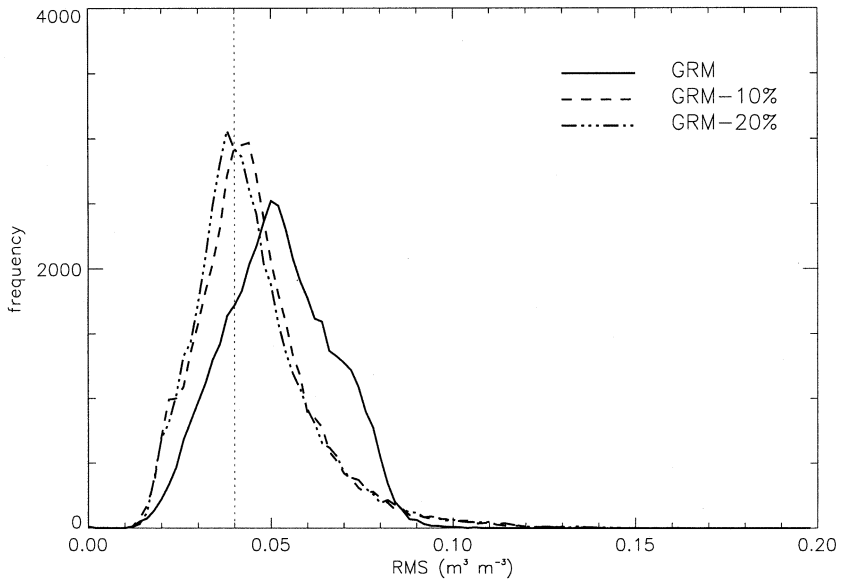

Fig. 5. Probability density function of the rms error on the retrieved surface soil moisture, at 0600 LST, for GRM (8), GRM (8)-10% and GRM (8)-20%, over 80% of the continental pixels, for a 1-K noise level and in 1988.

as continental pixels. As in the previous section, LRM was derived from the indexes given in Table III. Many LRM based on different combinations of indexes were tested on 15 contrasting pixels, including vegetated pixels, mixed pixels, bare soil pixels, etc. The approach consisted in training each LRM on 1987 and applying the obtained LRM to 1988, on 730 points (365 days $\times$ 2 times a day). These attempts showed that, conversely to the GRM approach where three indexes were used, the use of only two indexes ($AR_{V,50,20}$ and PR_{50}) was sufficient for an accurate LRM soil moisture retrieval. The LRM model was expressed as

$$wg^* = a_0 + a_1 AR_{V,50,20} + a_2 PR_{50}. \quad (9)$$

As a regression model was calibrated over each pixel, the specificity of each pixel (in terms of land cover, water percentage, soil texture, etc.) is implicitly accounted for in the regression coefficients of the LRM.

A. Applying LRM Over Four Selected Pixels

The results of this statistical retrieval algorithm are illustrated in Fig. 6 over four pixels during 1988, for a 1-K noise level configuration. The four selected pixels are the same as those used in Section IV. In Fig. 6, the time variations of both reference and retrieved soil moisture are compared. For the first pixel, located in the Mongolian plain, it can be seen that, conversely to the GRM approach, the soil moisture retrieval is feasible

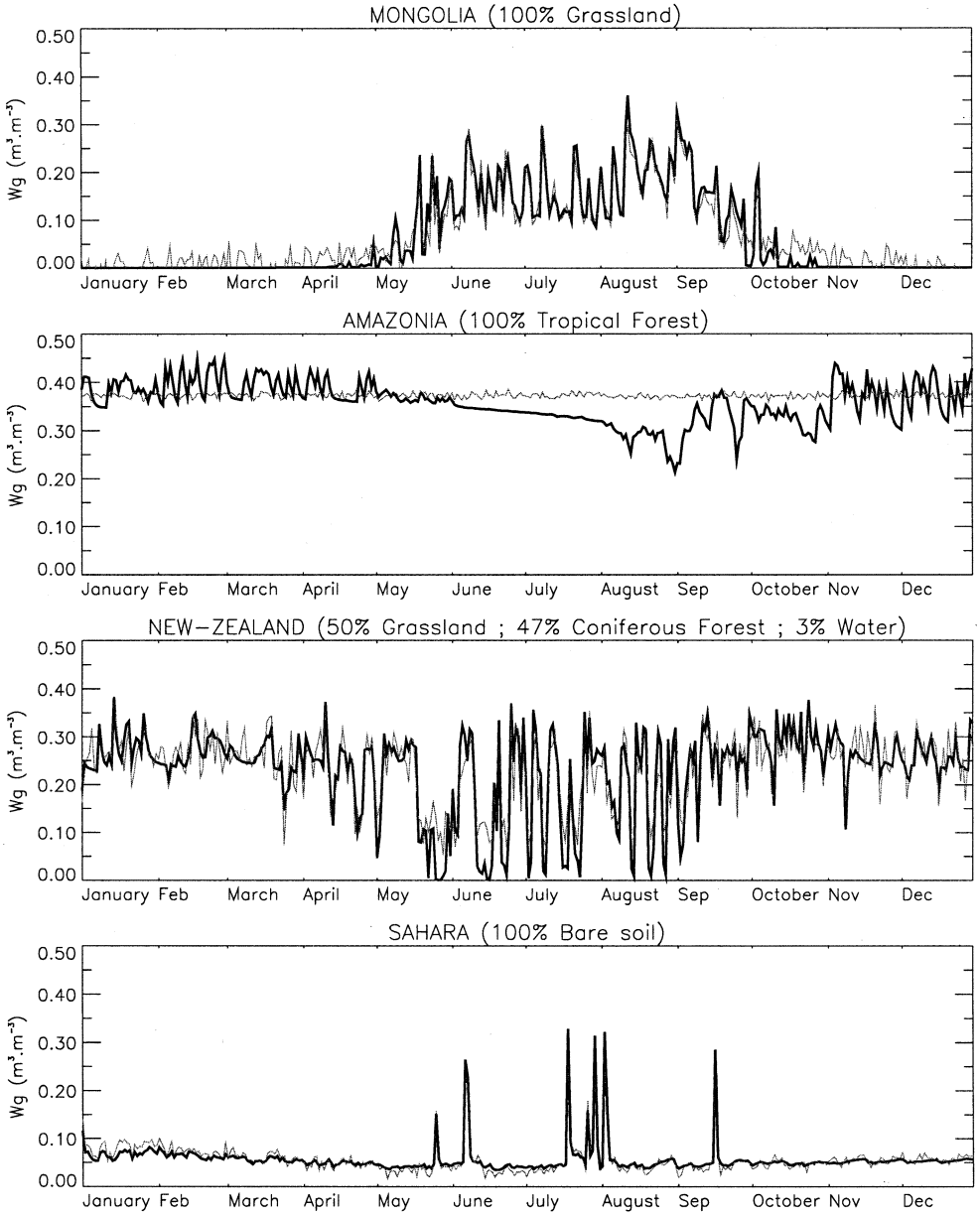

Fig. 6. Four examples of the annual time variations of the reference and LRM-estimated surface soil moisture (thick and thin lines, respectively), for a 1-K noise level, in 1988, at 0600 LST.

when the soil is frozen and snow is present, from November to April. Frozen soil conditions are rather similar to those of dry soils, since there is no liquid water in the first centimeters of the soil surface. Very good retrieval results were obtained over this pixel, since the rms error is equal to 0.017 $m^3 \cdot m^{-3}$, and the efficiency is 0.963. The microwave emission of the Amazonian pixel did not vary much. Therefore, the added noise on T_B corresponds to a small variation in T_B, but it was interpreted by the retrieval process as a sudden increase or decrease of the surface soil moisture. To reduce the sensitivity of the retrieved values to the added noise, the statistical method adjusted the coefficients a_1 and a_2 so as to reduce the influence of PR_{50} and $AR_{V,50,20}$ in the regression model [namely, low values of both a_1 and a_2 coefficients were obtained in (9)]. Over dense forests, the obtained LRM tends toward the mean reference soil moisture value, with therefore an efficiency value close to zero. As the time variations of the reference soil moisture are weak in Amazonia, the rms error of the retrieval in 1988 is rather low (0.045 $m^3 \cdot m^{-3}$). Also, in Fig. 6, retrievals are shown for the New Zealand mixed pixel. As for the Mongolian pixel, good retrieval results were obtained. Note, however, that the retrieval results were not accurate during some time periods in winter (from May to September). It seems that the lower accuracy obtained during soil freezing periods is due to the pixel heterogeneity (with 50% of coniferous forest), while the Mongolian pixel was homogeneous. In spite of the soil freezing periods, good retrievals were obtained over the New Zealand pixel (the mean rms error and the efficiency are equal to 0.036 $m^3 \cdot m^{-3}$ and 0.841, respectively). Finally, accurate surface soil moisture retrievals were obtained over the arid Saharan pixel. The calculated rms error and the efficiency are equal to 0.010 $m^3 \cdot m^{-3}$ and 0.913, respectively.

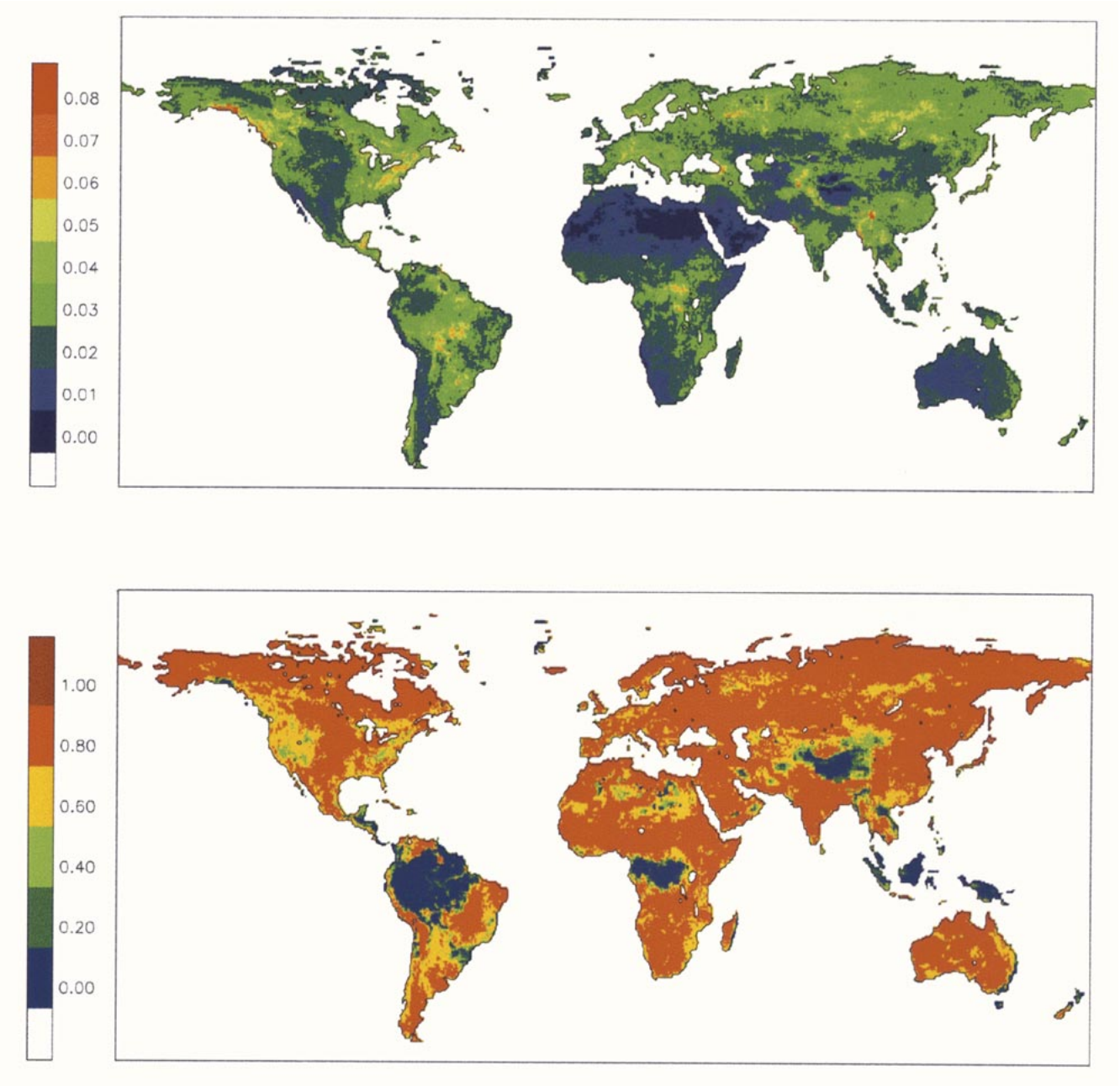

Fig. 7. Spatial distribution of the scores in soil moisture retrievals using LRM (9), for a 1-K noise level, in 1988, at 0600 LST. (Top) Root mean square error. (Bottom) model skill score.

B. Applying LRM at the Global Scale

The spatial distribution of both rms error and efficiency are given in Fig. 7 at the global scale. Using LRM at the 1-K noise level, the accuracy of the soil moisture retrievals is better than 0.04 $m^3 \cdot m^{-3}$ over about 90% of the global continental area for both years. However, it can be noted that many pixels present a near-zero efficiency. These pixels correspond to either dense vegetation attenuating the soil emission (like forested pixel), or to an extreme stability of the value of the surface soil moisture. In the first case, the rms error is high, denoting the weak sensitivity of the signal to soil moisture. In the second case, the rms error is low; but the LRM does not perform better than a model, which would prescribe the average soil moisture value, and a negative efficiency is obtained. This phenomenon was observed in the Tibet region and locally in some desert areas (Sahara, Iran, etc.).

A synthetic comparison of LRM with GRM is presented in Fig. 8. The probability density function of the rms error corresponding to LRM and GRM-20% for 1987 and 1988 is presented. It can be seen that 1) the global error distributions for 1987 and 1988 are similar for both methods, and 2) the use of LRM gives much better results than GRM-20%. With LRM, the $\overline{\text{rms}}$ value is equal to 0.029 $m^3 \cdot m^{-3}$ in 1987 and 0.030 $m^3 \cdot m^{-3}$ in 1988 (see also Table VII). As mentioned before, the accuracy of the LRM soil moisture retrieval is better than 0.04 $m^3 \cdot m^{-3}$ over about 90% of the global continental area for both years, while this proportion is only about 40% for GRM-20%, for a noise level of 1 K.

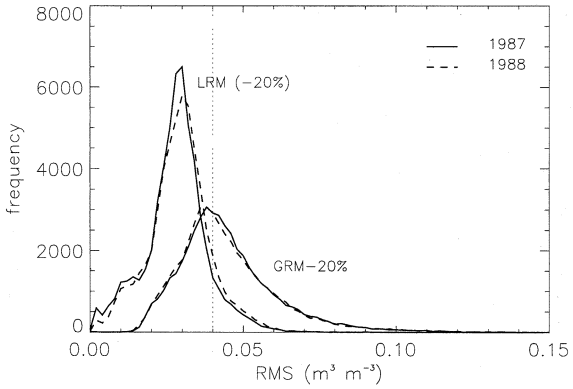

Fig. 8. Probability density function of the rms error on surface soil moisture (1987 and 1988), at 0600 LST, for LRM (9) and GRM (8)-20% (1-K noise level).

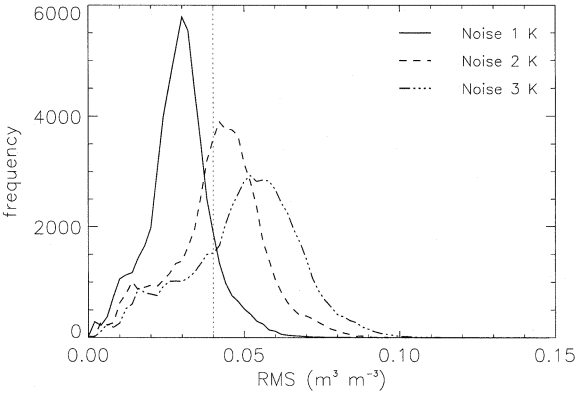

Fig. 9. Probability density function of the rms error on the retrieved surface soil moisture at 0600 LST, for LRM (9), for three different noise levels (1, 2, and 3 K). Note that different values of the a_0, a_1, and a_2 coefficients of the LRM (9) were computed over each pixel for the three noise levels.

The effect of the radiometric noise on the distribution of the LRM global rms error on surface soil moisture is evaluated in Fig. 9. It can be seen that the accuracy of the soil moisture retrieval is strongly sensitive to the noise which is added to the T_B values. Even for a 2-K noise level, the distribution of the rms error is significantly shifted toward high values. For this noise level, the proportion of continental pixels where the accuracy of the LRM retrieval is better than 0.04 $m^3 \cdot m^{-3}$ decreases significantly from 90% to less than 30%. This result indicate that the radiometric noise is one of the key parameters which will determine the instantaneous retrieval capability of the future L-band spaceborne microwave sensors.

It is also instructive to observe the spatial distribution of the regression coefficients a_0, a_1, and a_2 of the LRM over the globe. This distribution is illustrated in Fig. 10, and it can be seen that these coefficients seem to be well related to the thematic maps used in the forward simulation of the T_B data (i.e., Fig. 1). For example, the deserts and the forested areas can be distinguished in the a_0, a_1, and a_2 maps. However, a thorough analysis of the relationship between the LRM coefficients and the surface characteristics shows that these coefficients cannot be aggregated simply. An attempt was made to group the coefficients by considering a limited number of land covers (i.e., forested area, grassland, bare soil, etc.). The same average coefficient value was prescribed to a given surface type, and a linear mixing of the coefficients was applied to the mixed pixels. Therefore, a new spatial distribution of a_0, a_1, and a_2 values was obtained (not shown), and the new LRM coefficients were used to retrieve the surface soil moisture. The obtained accuracy of this reduced LRM was comparable to that of GRM-20%, i.e., much less than the full LRM. Indeed, the detailed LRM coefficients implicitly account for complex processes (surface characteristics, subpixel heterogeneity, the occurrence of rain, snow, and freezing periods, etc.), which is out of reach of simpler methods.

Finally, we have investigated the fact that an orbiting sensor does not look always at the same field of view, which may be a limitation of LRM. It was assumed that a linear interpolation of the LRM coefficients, combining the coefficients of the considered pixel with those of the neighboring pixels, could account for varied footprint positions. Position changes of 20% and 50% of the grid (i.e., about 10 and 25 km, respectively), both southward and eastward, were simulated for all the pixels by producing new sets of a_0, a_1, and a_2 coefficients. This new spatial distributions of the coefficients were applied to the initial maps of the indexes used in LRM (9). The new $\overline{\text{rms}}$ values were only slightly higher than using the original coefficients (0.032 and 0.038 $m^3 \cdot m^{-3}$, respectively, instead of 0.030 $m^3 \cdot m^{-3}$, in a 1-K noise level configuration). This result shows that errors in the field-of-view location have a limited impact on the quality of the retrievals and that LRM is a rather robust methodology.

C. Applying LRM to Local T_B Observations

The LRM relationship (9) was derived from the global T_B simulations produced by [13]. Therefore, this result was purely theoretical, and it was interesting to assess the robustness of the approach by applying it to observed L-band multiangular T_B. The PORTOS-93 data obtained by Wigneron *et al.* [9] over a wheat field during the whole growing period, and for varying soil moisture conditions, was used. The PORTOS instrument could perform multifrequency observations of T_B, including L-band. During the PORTOS-93 experiment, a number of agricultural surfaces in Avignon, southeastern France, were regularly observed with PORTOS at several incidence angles, along with gravimetric measurements of the surface soil moisture. The PORTOS T_B were not accurate, especially for the low frequencies. The radiometer absolute accuracy was about 3 K at 23.8 GHz, and although a precise value of the accuracy could not be estimated for the other channels of the instrument, it is expected that errors higher than 3 K must be considered for the low frequencies.

In this study, LRM was applied to the PORTOS-93 data over a growing wheat field [9]. Twenty-four T_B measurements presented the configuration required to calculate the two indexes $AR_{V,50,20}$ and PR_{50} used in (9). Table VIII compares the obtained coefficients with the average values of those produced in Section V-B for cropland pixels in Europe. The coefficient values obtained for PORTOS-93 indicate that the measurements were affected by rather large errors. For example, the average value of a_1 of European croplands decreased from about six to four for noise levels of 1 and 3 K, respectively, and a value of about two was obtained from PORTOS-93 (Table VIII). Fig. 11 presents a comparison between the measured wg and the estimation provided by LRM using either the average coefficients at

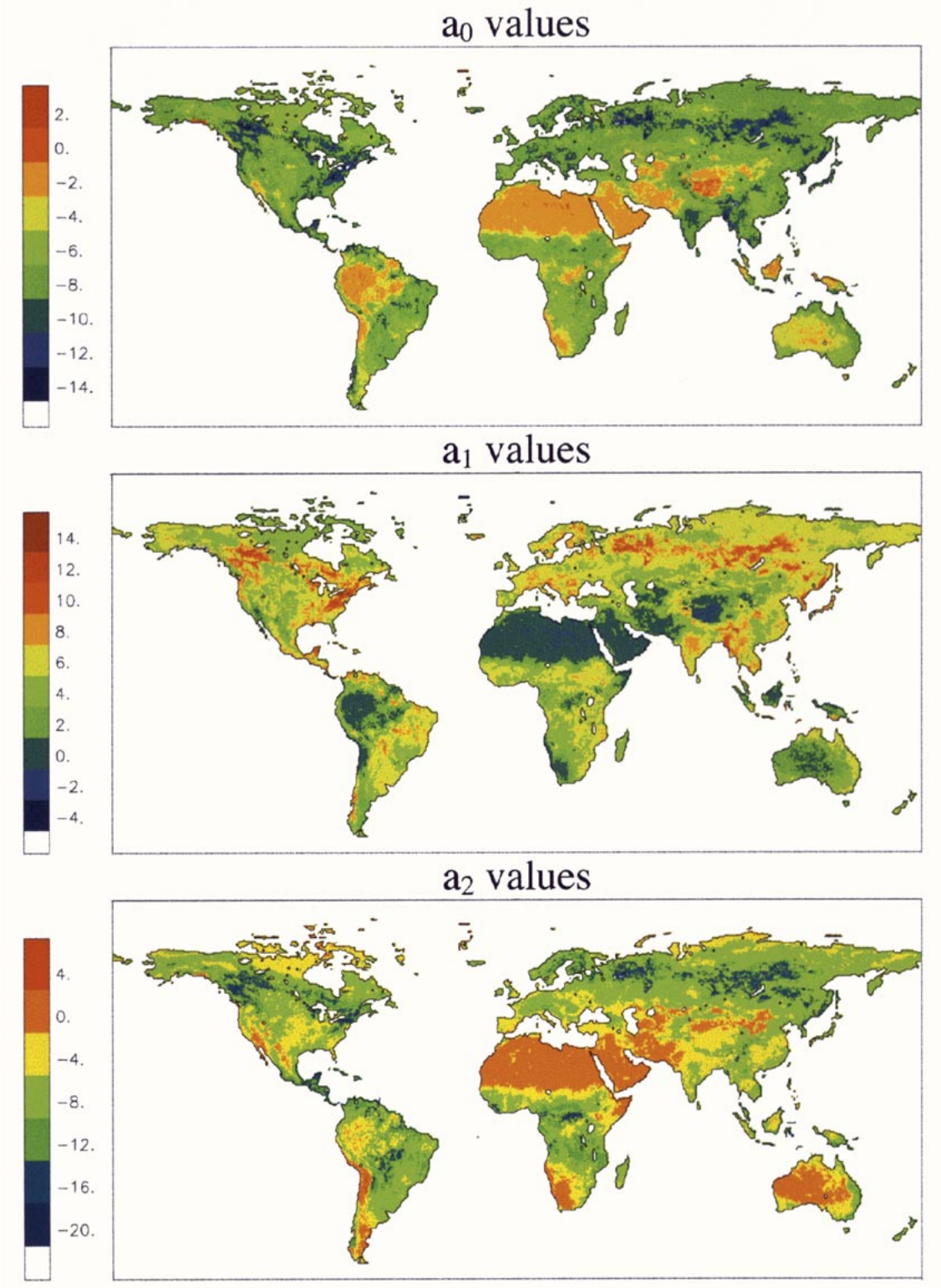

Fig. 10. Spatial distribution of the regression coefficients of LRM (9).

a noise level of 3 K or the best fit coefficients derived from the PORTOS-93 data. LRM performs well, since the R^2 and rms error values are 0.69 and 0.046 $m^3 \cdot m^{-3}$, respectively, using the best fit coefficients, and 0.68 and 0.066 $m^3 \cdot m^{-3}$, respectively, using the average coefficients corresponding to a 3-K noise level.

D. Comparison With Other Methods

Jackson *et al.* [6] have shown that an accuracy of 0.02–0.03 $m^3 \cdot m^{-3}$ on surface soil moisture retrieval could be obtained on grassland by using data from an airborne L-band radiometer, in southwestern Oklahoma. Measurements were acquired for a single incidence angle of 35° (normalized to

TABLE VIII
AVERAGE VALUES OF THE COEFFICIENTS OF LRM (9) DETERMINED FROM THE GLOBAL L-BAND T_B SIMULATIONS FOR CROPLANDS IN EUROPE (24 HALF-DEGREE PIXELS CONTAINING MORE THAN 90% OF CROPS) FOR THREE LEVELS OF INSTRUMENTAL NOISE (1, 2, AND 3 K), AND ESTIMATED FROM THE *IN SITU* L-BAND T_B MEASUREMENTS OF PORTOS-93 FOR A GROWING WHEAT FIELD

Area	Measurement error (K)	a_0	a_1	a_2
European croplands	1	-6.10 ± 0.51	6.05 ± 0.48	-3.41 ± 0.57
European croplands	2	-5.04 ± 0.56	5.02 ± 0.59	-2.83 ± 0.91
European croplands	3	-3.91 ± 0.63	3.94 ± 0.67	-2.24 ± 1.16
Wheat field (PORTOS-93)	3 or higher	-2.16	2.19	-0.73

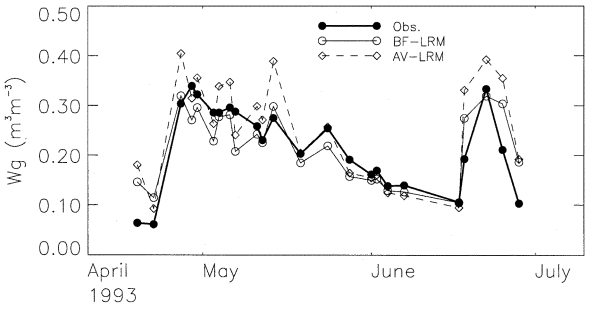

Fig. 11. Application of LRM (9) to PORTOS-93 data. The temporal evolution of observations (Obs.) of the surface water content of the top (0–50 mm) soil layer of a wheat field (wg) is compared with time series produced by LRM using either best fit coefficients (BF-LRM) or average coefficients (AV-LRM) for European croplands, for a noise level of 3 K (Table VIII).

nadir) and in horizontal polarization. Vegetation water content was either measured at various locations on the ground during the field campaign or estimated using normalized difference vegetation index (NDVI). The obtained accuracy is in agreement with our results in the same region. Using LRM (9) over four pixels centered on 98° W, 36° N, i.e., an area of about 10 000 km^2, the obtained mean rms error on soil moisture is 0.026 m$^3\cdot$ m^{-3} in a 1-K noise level configuration, and 0.042 and 0.054 m$^3\cdot$ m^{-3} for 2 and 3 K, respectively.

An evaluation of the Advanced Microwave Scanning Radiometer (AMSR) capabilities was made by Njoku and Li [10] over land surfaces. Three-parameter (soil moisture, soil temperature, and vegetation water content) retrievals were carried out from six channels of radiometric data (dual-polarized microwave brightness temperatures at 6.9, 10.7, and 18.7 GHz). The general methodology consisted in inverting a $\tau - \omega$ type model using an iterative least squares minimization technique. For an assumed noise of 0.3 K in all channels, a soil moisture retrieval accuracy of 0.06 m$^3\cdot$ m^{-3} could be obtained in regions where the vegetation water content was less than approximately 1.5 kg m^{-2}. In our context, regarding all pixels, which are not composed of a fraction of either forest or water, the mean rms error on soil moisture retrieval is 0.025 m$^3\cdot$ m^{-3} in a 1-K noise level configuration, and 0.031 and 0.036 m$^3\cdot$ m^{-3} for 2 and 3 K, respectively. Better results are likely to be obtained at L-band than at higher frequencies because of the enhanced sensitivity to soil moisture.

VI. DISCUSSION AND CONCLUSION

Two statistical models were developed and evaluated in order to retrieve the surface soil moisture using multiangular polarized L-band T_B. The global regression model consisted of a single relationship over the whole globe, whereas a different local regression model was obtained for each pixel. Modified versions of GRM were obtained over 90% and 80% of the continental surfaces (methods referred to as GRM-10% and GRM-20%), by excluding 10% and 20% of the worst pixels in terms of rms error on retrieved wg^*. The performance of these different statistical retrieval algorithms was evaluated for several levels of the instrumental noise (1, 2, and 3 K).

- For a 1-K noise level, it was found that best retrieval results were obtained by using the LRM. This method provided much better results than GRM-20%. The mean global rms error value of LRM is 0.029 and 0.030 m$^3\cdot$ m^{-3} in 1987 and 1988, respectively, The accuracy of the LRM soil moisture retrieval is better than 0.04 m$^3\cdot$ m^{-3} over about 90% of the global continental area for both years, while this proportion is only about 40% for GRM-20%.
- Both GRM and LRM approaches were found to be strongly sensitive to the noise level. For a 2-K noise level, the proportion of continental pixels where the accuracy of the LRM soil moisture retrieval is better than 0.04 m$^3\cdot$ m^{-3} decreased significantly from 90% to less than 30%.
- Noise levels higher than 2 K are significantly detrimental to the quality of the soil moisture retrievals presented in this study. However, as mentioned in the introduction, the SMOS radiometer measurements will be redundant [14], and signal processing techniques may enable one to attain the 1-K noise level.
- The LRM approach was applied to field measurements and produced relatively good estimates of the surface soil moisture.

The spatial distribution of the a_1, a_2, and a_3 coefficients used in the LRM method were found to be somewhat related to the thematic maps used in the forward simulation. However, it is unlikely that semiempirical relationships could relate, simply, these coefficients to the surface characteristics. These two aspects (sensitivity to the noise level, and relationships between the regression coefficients and the surface characteristics) should be investigated further in future studies.

Finally, it must be reminded that several sources of error may affect the employed global T_B dataset. In particular, the surface soil moisture, temperature, and snow characteristics provided by ISBA, forced by the ISLSCP I atmospheric data, may locally be different from the reality. The L-MEB model was extensively validated for crops, but errors in the simulated L-band emission are to be expected for natural vegetation and mountainous terrain. This model error constitutes an additional uncertainty which was not explicitly accounted for in this study.

ACKNOWLEDGMENT

The authors wish to thank the European Space Agency (ESA) and the Centre National d'Etudes Spatiales (CNES) for sup-

porting this work, as well as M. Berger, L. Simmonds, P. Waldteufel, J. Noilhan, and C. Prigent for helpful comments.

REFERENCES

[1] J. Noilhan and J.-C. Calvet, "Mesoscale land-atmosphere models and data needs," in *Proc. Passive Microwave Remote Sensing of Land-Atmosphere Interactions, ESA/NASA Int. Workshop*, St. Lary, 1993, pp. 17–54.

[2] E. F. Wood, D.-S. Lin, P. A. Troch, M. Mancini, and T. J. Jackson, "Soil moisture estimation: Comparisons between hydrologic model estimates and remotely sensed estimates," in *Proc. Passive Microwave Remote Sensing of Land-Atmosphere Interactions, ESA/NASA Int. Workshop*, St. Lary, 1993, pp. 17–54.

[3] J.-C. Calvet and J. Noilhan, "From near-surface to root-zone soil moisture using year-round data," *J. Hydrometeorol.*, vol. 1, no. 5, pp. 393–411, 2000.

[4] T. J. Schmugge and T. J. Jackson, "Mapping soil moisture with microwave radiometers," *Meteorol. Atmos. Phys.*, vol. 54, pp. 213–223, 1994.

[5] E. G. Njoku and D. Entekhabi, "Passive microwave remote sensing of soil moisture," *J. Hydrology*, vol. 184, pp. 101–129, 1996.

[6] T. J. Jackson, D. M. Le Vine, A. Y. Hsu, A. Oldak, P. J. Starks, C. T. Swift, J. D. Isham, and M. Haken, "Soil moisture mapping at regional scales using microwave radiometry: The Southern Great Plains Hydrology Experiment," *IEEE Trans. Geosci. Remote Sensing*, vol. 37, pp. 2136–2150, Sept. 1999.

[7] Y. H. Kerr, P. Waldteufel, J.-P. Wigneron, J. Font, and M. Berger, "Soil moisture retrieval from space: The Soil Moisture and Ocean Salinity (SMOS) Mission," *IEEE Trans. Geosci. Remote Sensing*, vol. 39, pp. 1729–1735, Aug. 2001.

[8] T. J. Jackson, D. M. Le Vine, C. T. Swift, T. J. Schmugge, and F. R. Schiebe, "Large area mapping of soil moisture using the ESTAR passive microwave radiometer in Washita'92," *Remote Sens. Environ.*, vol. 53, pp. 27–37, 1995.

[9] J. P. Wigneron, A. Chanzy, J.-C. Calvet, and N. Bruguier, "A simple algorithm to retrieve soil moisture and vegetation biomass using passive microwave measurements over crop fields," *Remote Sens. Environ.*, vol. 51, pp. 331–341, 1995.

[10] E. G. Njoku and L. Li, "Retrieval of land surface parameters using passive microwave measurements at 6-18 GHz," *IEEE Trans. Geosci. Remote Sensing*, vol. 37, pp. 79–93, Jan. 1999.

[11] M. Owe, R. de Jeu, and J. Walker, "A methodology for surface soil moisture and vegetation optical depth retrieval using the microwave polarization difference index," *IEEE Trans. Geosci. Remote Sensing*, vol. 39, pp. 1643–1654, Aug. 2001.

[12] J.-P. Wigneron, P. Waldteufel, A. Chanzy, J.-C. Calvet, and Y. Kerr, "Two-D microwave interferometer retrieval capabilities of over land surfaces (SMOS Mission)," *Remote Sens. Environ.*, vol. 73, pp. 270–282, 2000.

[13] T. Pellarin, J.-P. Wigneron, J. C Calvet, M. Berger, H. Douville, P. Ferrazzoli, Y. H. Kerr, E. Lopez-Baeza, J. Pulliainen, L. P. Simmonds, and P. Waldteufel, "Two-year global simulation of L-band brightness temperatures over land," *IEEE Trans. Geosci. Remote Sensing*, vol. 39, July 2003.

[14] P. Waldteufel, E. Anterrieu, J. M. Goutoule, and Y. Kerr, "Field of view characteristics of a microwave 2-D interferometric antenna, as illustrated by the MIRAS concept," in *Microwave Radiometry and Remote Sensing of the Earth's Surface and Atmosphere*, P. Pampaloni and S. Paloscia, Eds. Utrecht, The Netherlands, 2000, pp. 477–483.

[15] J. Noilhan and S. Planton, "A simple parameterization of land surface processes for meteorological models," *Mon. Weather Rev.*, vol. 117, pp. 536–549, 1989.

[16] B. W. Meeson, F. E. Corprew, J. M. P. McManus, D. M. Myers, J. W. Closs, K.-J. Sun, D. J. Sunday, and P. J. Sellers, *ISLSCP Initiative I-Global Data Sets for Land-Atmosphere Models*: NASA, 1995, vol. 1–5.

[17] V. Masson, J. L. Champeaux, F. Chauvin, C. Meriguet, and R. Lacaze, "A global database of land surface parameters at 1 km resolution in meteorological and climate models," *J. Climate*, vol. 16, no. 9, pp. 1261–1282, 2003.

[18] J. Pulliainen and M. Hallikainen, "Retrieval of regional snow water equivalent from space-borne passive microwave observations," *Remote Sens. Environ.*, vol. 75, pp. 76–85, 2001.

[19] T. J. Jackson and T. J. Schmugge, "Vegetation effects on the microwave emission of soils," *Remote Sens. Environ.*, vol. 36, pp. 203–212, 1991.

[20] P. Ferrazzoli, L. Guerriero, and L. J-P Wigneron, "Simulating L-band emission of forests in view of future satellite applications," *IEEE Trans. Geosci. Remote Sensing*, vol. 40, pp. 2700–2708, Dec. 2002.

[21] Y.-A. Liou, S. F. Liu, W. J. Wang, J.-P. Wigneron, and J. B. Lee, "Retrieval of crop biomass and soil moisture from measured 1.4 and 10.65 GHz brightness temperatures," *IEEE Trans. Geosci. Remote Sensing*, vol. 40, pp. 1260–1268, June 2002.

[22] J. R. Wang, J. E. McMurtrey, E. T. Engman, T. J. Jackson, T. J. Schmugge, W. I. Gould, J. E. Fuchs, and W. S. Glazar, "Radiometric measurements over bare and vegetated fields at 1.4-GHz and 5-GHz frequencies," *Remote Sens. Environ.*, vol. 12, pp. 295–311, 1982.

[23] W. L. Teng, J. R. Wang, and P. C. Doraiswamy, "Relationship between satellite microwave radiometric data, antecedent precipitation index, and regional soil moisture," *Int. J. Remote Sens.*, vol. 14, no. 13, pp. 2483–2500, 1993.

[24] A. Chanzy, T. J. Schmugge, J.-C. Calvet, Y. Kerr, P. van Oevelen, O. Grosjean, and J. R. Wang, "Airborne microwave radiometry on a semi-arid area during Hapex-Sahel," *J. Hydrol.*, vol. 188–189, pp. 285–309, 1997.

[25] J.-P. Wigneron, J.-C. Calvet, T. Pellarin, A. van de Griend, M. Berger, M. A Chanzy, P. Ferrazzoli, and L. Simmonds, "Retrieving soil moisture from microwave radiometric observations: Current status and future plans," *Water Resources Res.*, vol. 85, no. 4, pp. 489–506, 2003.

[26] D. M. Le Vine and S. Abraham, "The effect of the ionosphere on remote sensing of sea surface salinity from space: Absorption and emission at L-band," *IEEE Trans. Geosci. Remote Sensing*, vol. 40, pp. 771–782, Apr. 2002.

[27] S. H. Yueh, "Estimates of Faraday rotation with passive microwave polarimetry for microwave remote sensing of earth surfaces," *IEEE Trans. Geosci. Remote Sensing*, vol. 38, pp. 2434–2438, Sept. 2000.

Thierry Pellarin was born in Versailles, France, in 1972. He received the Ph.D. degree from the University of Grenoble, Grenoble, France, in 2001.

In 2001, he joined Météo-France/CNRM, Toulouse, France. His current main field of interests is in microwave radiometry, with particular emphasis on the Soil Moisture and Ocean Salinity (SMOS) Project. His thesis work concerned the use of weather radars for hydrological applications in mountainous regions.

Jean-Christophe Calvet received the engineering degree in agronomy from the Institut National Agronimique Paris-Grignon, Paris, France, and the engineering degree in meteorology from the Ecole Nationale de la Météorologie, Toulouse, France.

In 1990, he joined Météo-France/CNRM, Toulouse, France, and has been working in the field of remote sensing and land surface modeling, for applications in meteorology. His most recent works concern the analysis of soil moisture and the representation of an interactive vegetation in climate models. He was involved with the scientific team of the Soil Moisture and Ocean Salinity (SMOS) project. He has contributed to the development of the SMOS land parameter retrieval algorithms, to field experiments to validate the SMOS products, and to the demonstration of the possibility to assimilate SMOS data into land surface models.

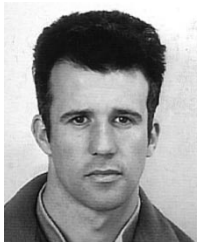

Jean-Pierre Wigneron (M'97) received the engineering degree from SupAéro, ENSAE, Toulouse, France, and the Ph.D. degree from the University of Toulouse, Toulouse, France, in 1993.

He is currently a Research Scientist at INRA, Bordeaux, France. His research interests are in microwave remote sensing of soil and vegetation, radiative transfer, and data assimilation. He is currently developing microwave models and soil moisture retrieval approaches in the framework of the Soil Moisture and Ocean Salinity (SMOS) Mission. He was Principal and Co-Investigator of several ground and airborne international campaigns in the field of microwave remote sensing (PORTOS-93, PORTOS-96, RESEDA, SMOS-99, and EUROSTARRS).